The Wicking Kinetics of Liquid Droplets into Yarns

XUEMIN CHEN, KONSTANTIN G. KORNEV, YASH K. KAMATH, AND ALEXANDER V. NEIMARK[1]

TRI/Princeton, P.O. Box 625, Princeton, New Jersey 08542, U.S.A.

ABSTRACT

The wicking kinetics of liquid droplets into yarns is studied using a computerized imaging system. A new method is suggested for characterizing the yarn structure by monitoring droplet absorption. The method is based on the comparative analysis of the time needed for droplet disappearance as a function of droplet volume for various yarns. A mathematical model is developed to describe the wicking kinetics. We show that for wetting liquids, the time of droplet absorption T_w is a linear function of the initial droplet volume squared V_0^2. For a given liquid-yarn pair, the slope of this relationship provides important information about the yarn properties. The linear relationship between T_w and V_0^2 is verified by experimental data for a typical spin finish. The model predicts that droplet wicking can occur even if the advancing contact angle θ_a is slightly greater than 90°. However, for nonwetting liquids, the relationship between T_w and V_0^2 is nonlinear, and a criterion for droplet wicking into nonwetted yarns is obtained.

Textile fibers and yarns are often treated with spin finishes that act as lubricants and antistatic agents during processing. Deposited on the yarn surface, the finish liquid wicks into the interfiber space, thus providing filament cohesion and modifying yarn mechanical and chemical properties [12]. To process the yarns satisfactorily, absorption of the finish liquid must be sufficiently fast and uniform. To evaluate the performance of spin finishes or to characterize the wettability and structural properties of yarns, standard techniques of wicking are used [2, 4–8, 10, 13]. With these techniques, the yarn is either partially immersed in a liquid reservoir [3, 5, 7] or a constant supply of liquid is delivered to a certain point on the yarn [4]. The position of the liquid front is traced as a function of time. The relation between the liquid front position and the time of droplet wicking is assumed to be of the Lucas-Washburn type [6, 13],

$$L^2 = \frac{\gamma R \cos\theta_a}{2\eta} t \quad , \qquad (1)$$

where L is the liquid front position or wicking length, γ and η are the surface tension and viscosity of the liquid, respectively, θ_a is the apparent contact angle, R is the effective hydraulic radius of the interfilament pores, and t is time.

In this paper, we present a new method to study wicking in yarns by recording the time needed for the complete absorption of a droplet deposited on the yarn surface. We have developed a PC-based imaging system and a mathematical model to study the wicking of liquid droplets into yarns. The selected images in Figure 1 show the dynamics of a hexadecane droplet absorption in a polypropylene (PP) yarn. For a given liquid-yarn pair, the time of droplet disappearance depends only on the initial droplet volume. The mathematical model allows us to relate the time of droplet absorption to droplet volume. Unifying the wetting and nonwetting cases, the model operates with two driving forces responsible for wicking.

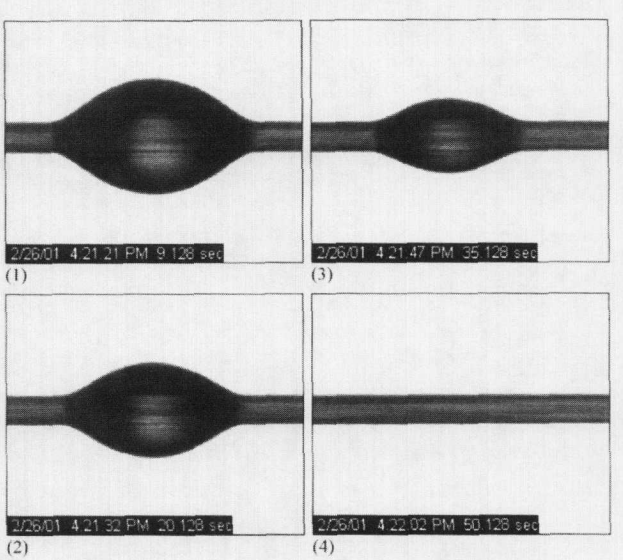

FIGURE 1. Selected images for the absorption of a hexadecane droplet in a polypropylene yarn.

[1] Author for correspondence: aneimark@triprinceton.org

The pressure drop at the liquid front causes imbibition of a wetting liquid and hinders the penetration of a nonwetting liquid. The Laplacian pressure difference due to droplet curvature facilitates liquid penetration for both wetting and nonwetting cases. Thus, the model generalizes the Washburn approach and enables us to obtain a quantitative criterion for droplet wicking. We test the model with experimental data to show its applicability to wicking of liquids in yarns.

Theory

THE MODEL

When deposited on a yarn, a droplet of wetting liquid spontaneously wicks into the yarn due to the capillary forces associated with the given structure and geometry of the void spaces between the filaments. The model describing the droplet disappearance focuses on the stage just after the yarn section underneath the droplet has been saturated with the liquid (Figure 2). When the droplet size is sufficiently small, the effect of gravity on the droplet shape is negligible and the droplet may be considered axisymmetric. Quantitatively, the approximation is valid if the characteristic length of the capillary wave $l_{cap} = \sqrt{\gamma/\rho g}$ is larger than the droplet radius R_d. Typically, parameter l_{cap} is on the order of a millimeter, so the smaller droplets are the objects of our study.

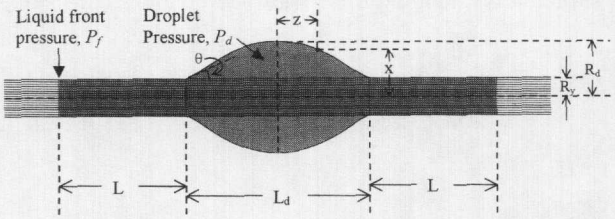

FIGURE 2. Schematic of the wicking process.

Movement of the liquid front along the yarn is caused by a pressure difference between the droplet P_d and the liquid front P_f. Since the process of liquid imbibition is slow, we can assume that the droplet takes an equilibrium shape at each instant of time. Then the pressures can be expressed by means of the droplet curvature $2H$ (see the Appendix for its definition) and the hydraulic radius of the yarn pores R as

$$P_d = P_g + (2H)\gamma \quad , \tag{2}$$

$$P_f = P_g - (2\gamma \cos \theta_a)/R \quad , \tag{3}$$

where P_g is the atmospheric pressure. Applying Darcy's law [5, 7, 11] for the flow rate, we have

$$\frac{dL}{dt} = \frac{k(P_d - P_f)}{\eta L} = \frac{2k\gamma(H + \cos \theta_a/R)}{\eta L} \quad , \tag{4}$$

where k is the permeability of the yarn. Equation 4 must be complemented by both a condition of mass conservation and an expression for the droplet curvature.

Condition of mass conservation: Assuming that the evaporation of the liquid is negligible and the liquid is incompressible, the mass balance can be written as

$$V_d + \varepsilon \pi R_y^2(L_d + 2L) = V_0 + \varepsilon \pi R_y^2 L_0 = V_{\text{total}} = \text{constant} \quad , \tag{5}$$

where V_d is the current droplet volume, L_d is the current droplet length (see Figure 2 and the Appendix for their definitions), V_0 and L_0 are the droplet volume and length at the initial instant of time $t = 0$, R_y is the yarn radius, V_{total} is the total liquid volume, and ε is the yarn porosity. Introducing the notations

$$\Delta V_d = V_d - V_0 \tag{6}$$

and

$$\Delta L_d = L_d - L_0 \quad , \tag{7}$$

the volume of liquid that has been absorbed by the yarn V_w can be expressed as

$$V_w = -\Delta V_d = \varepsilon \pi R_y^2(\Delta L_d + 2L) \quad . \tag{8}$$

Droplet curvature as a function of droplet volume: The equilibrium shape of a droplet can be specified by four parameters: the yarn radius R_y, the maximum radius of the droplet R_d, the droplet length L_d, and the contact angle at which the droplet meets the yarn θ [1] (see Figure 2). The formulas for droplet volume and droplet curvature can be found in the Appendix. Because of the dynamic nature of the wicking process and the complex geometry of the yarn surface, θ and θ_a may differ.

GENERAL SOLUTION

Making use of Equations 5–8 to express the moving front coordinate through the droplet volume and the droplet length as

$$L = -\frac{\Delta V_d + \varepsilon \pi R_y^2 \Delta L_d}{2\varepsilon \pi R_y^2} \quad , \tag{9}$$

and introducing the dimensionless droplet volume $\bar{V}_d$ and droplet length $\bar{L}_d$ as

$$\bar{V}_d = V_d/R_y^3, \quad \Delta \bar{V}_d = (V_d - V_0)/R_y^3 \quad , \tag{10}$$

$$\bar{L}_d = L_d/R_y, \quad \Delta\bar{L}_d = (L_d - L_0)/R_y \quad , \qquad (11)$$

we can rewrite Equation 4 in the form

$$(\bar{V}'_d + \varepsilon\pi\bar{L}'_d)\frac{dn}{dt} = \frac{8\varepsilon^2\pi^2 k\gamma}{\eta R_y^3(\Delta\bar{V}_d + \varepsilon\pi\Delta\bar{L}_d)}\left(\frac{n - \cos\theta}{n^2 - 1} + \alpha\right) \quad , \qquad (12)$$

where $n = R_d/R_y$, $\bar{V}'_d = d\bar{V}_d/dn$, $\bar{L}'_d = d\bar{L}_d/dn$, and the dimensionless parameter α is introduced as

$$\alpha = R_y \cos\theta_a/R \quad . \qquad (13)$$

Integration of Equation 12 within the limits $t = 0$ ($n = n_0$) and $t = T_w$ ($n = 1$) gives us the time of droplet absorption as

$$T_w = \frac{\eta R_y^3}{8\varepsilon^2\pi^2 k\gamma} \times \int_{n_0}^{1} \frac{(\bar{V}'_d + \varepsilon\pi\bar{L}'_d)(\Delta\bar{V}_d + \varepsilon\pi\Delta\bar{L}_d)(n^2 - 1)}{n - \cos\theta + \alpha(n^2 - 1)}\, dn \quad . \qquad (14)$$

Before proceeding to the physical interpretation of Equation 14, let us consider some limiting cases.

Wicking of Completely Wetting Liquids, $\alpha \gg 1$

In this case, we have $\cos\theta \approx 1$, and Equation 4 can be written as

$$\frac{dL}{dt} = \frac{2k\gamma}{\eta L R_y}\left(\frac{1}{n+1} + \alpha\right) \quad . \qquad (15)$$

The capillary pressure at the liquid front dominates the Laplacian pressure in the droplet. The first term in the right hand side of Equation 15 can be neglected as compared to the second one. If we assume that the capillaries in the yarn are cylindrical, then the permeability of the yarn can be expressed as $k = R^2/8$ [11], and we arrive at the asymptotic equation

$$\frac{dL}{dt} = \frac{\gamma R \cos\theta_a}{4\eta L} \quad . \qquad (16)$$

The solution to Equation 16 subject to the initial condition $L = 0$ at $t = 0$ is merely the Lucas-Washburn relation (Equation 1). In the experiments illustrated by Figure 1, the position of the liquid front or the wicking length cannot be detected when the liquid has propagated beyond the view area of the camera. However, the volume of liquid remaining in the droplet and the time of droplet disappearance can be determined from the image. Since the change in droplet length is much smaller than the wicking length, $\Delta L_d \ll 2L$, Equation 8 can be approximated as

$$V_w = 2\varepsilon\pi R_y^2 L \quad . \qquad (17)$$

Taking into account Equation 17, the Lucas-Washburn equation (1) can be converted into

$$V_w^2 = \frac{2\varepsilon^2\pi^2 R_y^4 \gamma R \cos\theta_a}{\eta} t \quad . \qquad (18)$$

Rewritten for the moment of droplet disappearance, Equation 18 can be used for the yarn characterization with respect to its ability to absorb the finish liquid:

$$T_w = \frac{\eta}{2\varepsilon^2\pi^2 R_y^4 \gamma R \cos\theta_a} V_0^2 \quad . \qquad (19)$$

Criterion for Wicking of Almost Nonwetting Liquids

The model under consideration can be extended to the case of nonwetting fluids as well. We again consider the situation when the yarn fragment just beneath the droplet is somehow saturated with the liquid. Based on Equation 4, the condition of droplet wicking in a yarn is $dL/dt > 0$. Expressing the droplet curvature through n and cos θ, we arrive at the condition for droplet wicking as

$$\frac{n - \cos\theta}{n^2 - 1} + \alpha > 0 \quad . \qquad (20)$$

As seen from Equation 20, the model predicts that wicking can still occur even if θ_a is greater than 90°, yet n is sufficiently small. Figure 3 shows the regions of wicking

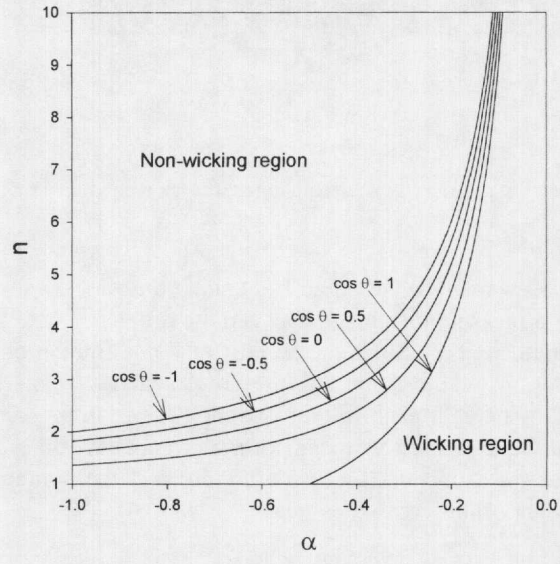

FIGURE 3. Wicking conditions or stability diagram for a droplet resting on a yarn.

and nonwicking for $-1 \leq \alpha \leq 0$. The right boundary for all the curves is $n \rightarrow \infty$ as $\alpha \rightarrow 0$. As seen from the stability diagram (Figure 3), for a given apparent contact angle θ_a, the wicking boundary is shifted to the left as the visible droplet contact angle θ increases. This is because of the increased Laplacian pressure associated with the adhering droplet. To guarantee droplet stability, the pore radius has to be decreased.

Analysis of the General Equation 14

Equation 14 provides the basic relationship governing the disappearance of a droplet on a yarn. It relates the time of droplet absorption to the initial droplet volume. The time depends on the physicochemical properties of the liquid (γ and η), the yarn and fiber wettabilities (cos θ and cos θ_a), and the geometric and structural properties of the yarn (k, ε, R, and R_y). Introducing the dimensionless wicking time as

$$\bar{T}_w = T_w \frac{8\varepsilon^2\pi^2 k\gamma}{\eta R_y^3} \quad , \tag{21}$$

Equation 14 is rewritten as

$$\bar{T}_w = \int_{n_0}^{1} \frac{(\bar{V}_d' + \varepsilon\pi\bar{L}_d')(\Delta\bar{V}_d + \varepsilon\pi\Delta\bar{L}_d)(n^2-1)}{n - \cos\theta + \alpha(n^2-1)}\, dn \quad . \tag{22}$$

The dimensionless wicking time is a function of four dimensionless parameters—n_0, θ, α, and ε. Since n_0 and θ determine $\bar{V}_0$, for the given yarn porosity the dimensionless wicking time can be expressed as a function of α and $\bar{V}_0$:

$$\bar{T}_w = f(\alpha, n_0, \theta) = f(\alpha, \bar{V}_0) \quad . \tag{23}$$

The dimensionless wicking time can be calculated by numerical integration of Equation 22. Due to the multiparameters of the basic equation, we focus on the case cos $\theta \approx 1$, which is more relevant to practical applications. The dimensionless time of droplet absorption $\bar{T}_w$ has been calculated for various values of n_0, α, and ε. In Figure 4, $\bar{T}_w$ is plotted as a function of n_0 and α for closely packed yarns ($\varepsilon = 0.1$). In Figure 5, $\bar{T}_w$ is drawn as a function of $\bar{V}_0^2$ for various α at the same porosity $\varepsilon = 0.1$. The dotted lines in Figure 5 represent the results calculated from the Lucas-Washburn equation (19) rewritten in the dimensionless form as $\bar{T}_w = \bar{V}_0^2/(2\alpha)$. For $\alpha \geq 1$ (wetting or partially wetting cases), the wicking process can be described by a linear relationship between $\bar{T}_w$ and $\bar{V}_0^2$. For this particular case ($\varepsilon = 0.1$), whenever $\alpha \geq 5$, the slopes of the straight lines are very close to those predicted by the Lucas-Washburn equation. For yarns of low wettability, the time of droplet absorption increases. Moreover, the kinetics of liquid

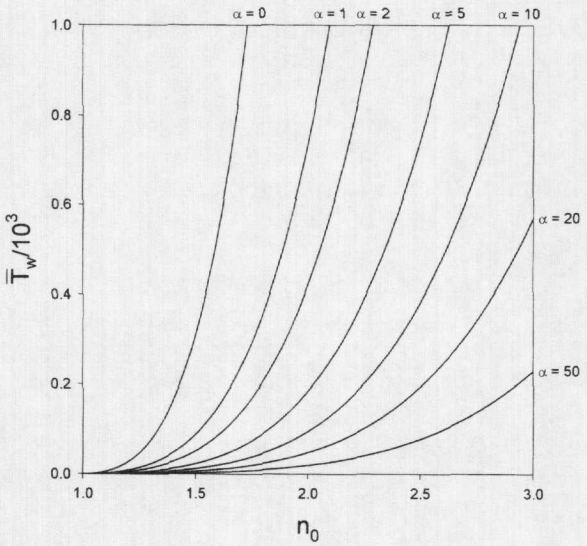

FIGURE 4. Dimensionless time of droplet absorption as a function of n_0 at $\varepsilon = 0.1$ and cos $\theta = 1$.

imbibition changes drastically. Decreasing α below one-half, the linear relation between $\bar{T}_w$ and $\bar{V}_0^2$ turns out to the nonlinear, thus manifesting the effect of yarn hydrophobicity (Figure 6).

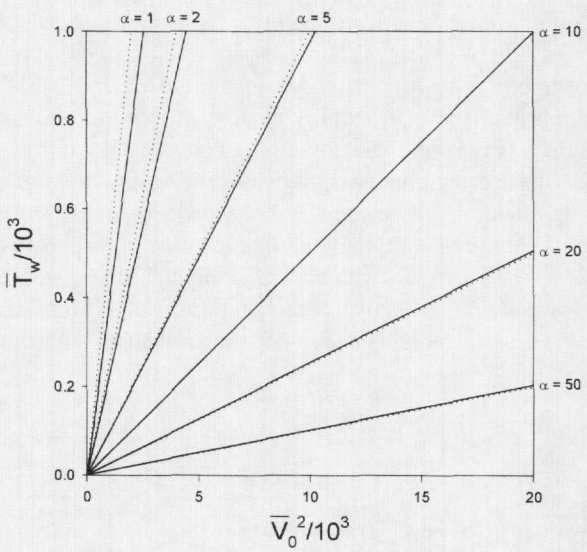

FIGURE 5. Dimensionless time of droplet absorption as a function of the dimensionless droplet volume squared, $\varepsilon = 0.1$, cos $\theta = 1$. The solid lines represent the results calculated from Equation 22. The dotted lines represent results calculated from the Lucas-Washburn equation.

Experimental

Our theory underlies the method of yarn characterization. A PC-based imaging system relates the model pa-

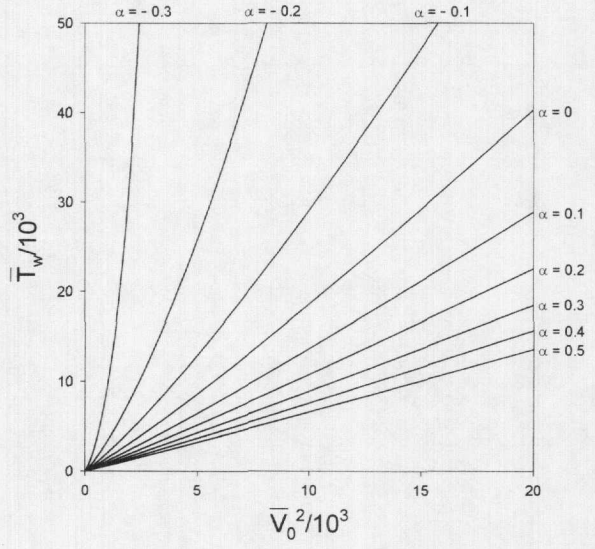

FIGURE 6. Dimensionless time of droplet absorption as a function of the dimensionless droplet volume squared for nonwetting situations at $\varepsilon = 0.1$ and $\cos\theta = 1$.

rameters with the measured ones. Figure 7 shows a schematic diagram of the imaging system, which consists of a high-speed digital CCD camera (Dalsa CA-D1-0256A) with a video zoom lens (Navitar Zoom 6000 or Zoom 7000), a power supply, an image acquisition board, the PC, a light source, and a fiber/yarn mounting assembly. The camera has a resolution of 256 × 256 pixels and is able to acquire images at a rate of up to 200 frames per second. The pixel sizes have been calibrated for different camera magnifications. At the minimum magnification, the camera has a view area of 30 × 30 mm^2. At the maximum magnification, one pixel is equivalent to 3.5 μm. The camera and computer are connected to provide image analysis in a real time scale. This set-up allows us to record the droplet shape changes and thus

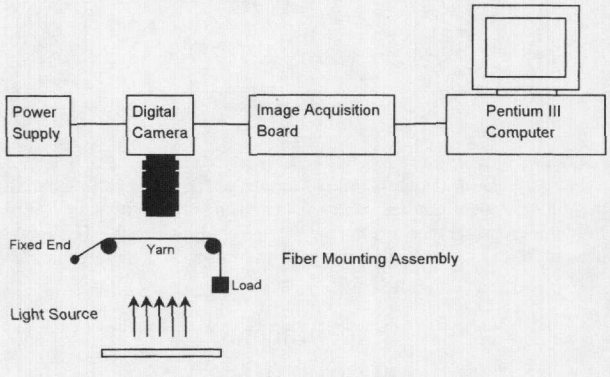

FIGURE 7. Schematic diagram of the PC-based imaging system.

the kinetics of droplet absorption. A detailed analysis of the absorption dynamics will be published elsewhere. In this paper, we focus on a simplified version of yarn characterization using limited information about the system. The input parameters of the proposed method are limited to the initial droplet volume and the time of droplet disappearance.

EXPERIMENTAL FEATURES

To illustrate the method, we consider the absorption of two liquids, hexadecane (Aldrich) and spin finish Lurol PP-912 (Goulston Technologies), into yarns of finish-free nylon fibers (200 denier) and of polypropylene fibers (200 denier). The properties of liquids and yarns are listed in Table I, where n_f is the number of fibers in the yarn and R_f is the fiber radius. The experiments are conducted at ambient temperature (20–25°C). The yarn is mounted horizontally on the frame. Fixing one end of the yarn and applying a load (typically 50 g) to the other end, we can keep the yarn taut.

TABLE I. Systems studied and properties of the liquids and yarns.

Liquid	Yarn	ρ, g/cm^3	γ, mN/m	η, cp	cos θ_a	n_f	R_f, μm
Hexadecane	nylon	0.773	27	3.3	1.000	32	14
Hexadecane	PP, #1	0.773	27	3.3	1.000	62	11
PP-912	PP, #2	1.06	30	38	0.837	33	15

After the yarn has been mounted in place, the view area, frame rate, light intensity, aperture, magnification, and focus are adjusted to the desired settings. The frame rate can be changed during an image acquisition session, depending on how fast the image changes. A liquid droplet is deposited on the yarn with a micro syringe, and the images are recorded as a function of time. The droplet size decreases as a result of wicking, and after a certain period of time, it disappears. The volume of the droplet at each moment of time is obtained from the images.

The range of droplet volumes typically varies from 0.1 to 1 mm^3. Although the volume of liquid can be measured with the microsyringe, the transfer of liquid from the syringe needle to the yarn is often incomplete, leaving a residual amount of liquid on the needle. Since the droplet volume can be found from the image, it is not necessary to control the initial liquid volume. However, in order to test the calculation method (see discussions below), the initial liquid volume has to be measured independently. In the reference measurements, we are extra careful to make the liquid transfer as complete as possible.

CALCULATING DROPLET VOLUME AND CONTACT ANGLE FROM IMAGES

Based on Caroll's solution for the droplet profile [1] (see Appendix), we have written a computer program to calculate the contact angle θ and droplet volume V_d from experimental images. The equations used in the calculations are given in the Appendix. To test the program, we have used a well-characterized system, a hexadecane droplet on a nylon fiber (see Figure 8). The calculation involves the following steps: (1) the profile fragments at the contact lines are extracted from the original image (Figure 8), (2) the edges are converted to a two-dimensional array (z, x) containing pixel positions, (3) the lines of symmetry are determined in the horizontal and vertical directions, (4) the droplet edges are folded along the lines of symmetry, and the average values of the horizontal length z and the radius x are calculated, (5) the droplet profile is determined by fitting the (z, x) curve using the contact angle as an adjustable parameter, and (6) the droplet volume is calculated using Caroll's formulas (see Appendix).

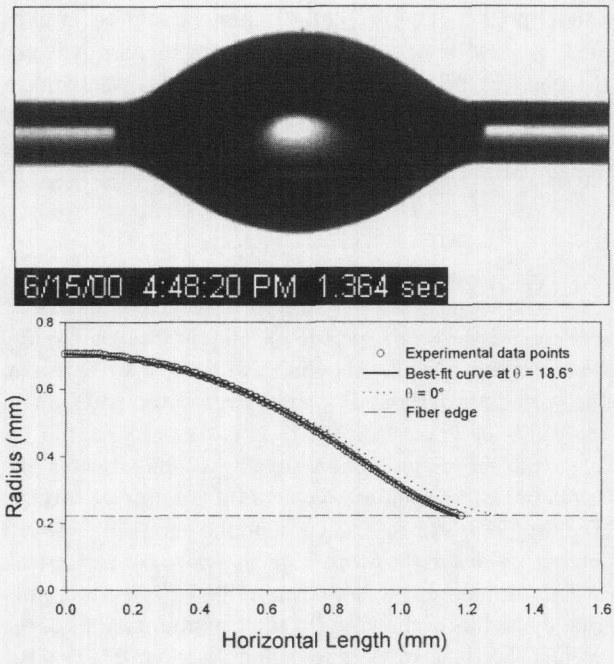

FIGURE 8. (a) A hexadecane droplet deposited on a nylon fiber. Droplet volume is 2 mm^3 and the fiber radius is 0.215 mm. (b) Droplet edges extracted from the original image.

Figure 8 shows the experimental and calculated droplet profiles. The best-fit profile is obtained if we put $\theta = 18.6°$, which gives $\cos\theta = 0.948$. This value is in agreement with that found by the Wilhelmy method [9]. The calculated droplet volume is $V_d = 1.92\ mm^3$, which is 4% smaller than the volume measured with the micro syringe used to transfer the liquid to the fiber. We have observed that a small amount of liquid remains on the syringe needle after the droplet is deposited onto the fiber. Most likely, this remainder gives rise to the difference in the volumes. Thus, the results show that the model provides a reasonably accurate method for calculating the droplet volumes from experimental images.

Results and Discussion

WICKING OF POLYPROPYLENE AND NYLON YARNS

Experiments on droplet disappearance can be used as a simple tool for analyzing yarn structure. For wetting situations, $\cos\theta_a = 1$, where α values are large, $\alpha \gg 1$, the capillary pressure at the liquid front is the dominant driving force for the wicking process. Equations 18 and 19 become the basic relationships governing droplet absorption by a yarn. Figure 1 shows selected images of the wicking of a hexadecane droplet in a polypropylene yarn (PP, #1). The contact angle between the droplet and the yarn is 0°, indicating a complete wetting situation. Figure 9 shows a plot of V_w^2 and the dimensionless droplet radius n as functions of time t. Selected images of this process are presented in Figure 1. The estimate of the parameters in Equation 14 is based on the definition of porosity as the ratio of void volume to the volume of the yarn. The former calculated per unit length of the yarn is $\pi R_y^2 - \pi n_f R_f^2$, while the latter is πR_y^2. Thus, the porosity of the yarn can be calculated as $\varepsilon = 1 - n_f(R_f/R_y)^2$. At the same time, the yarn radius R_y can be measured from the images. From the slope of the straight line, the effective capillary radius R can be

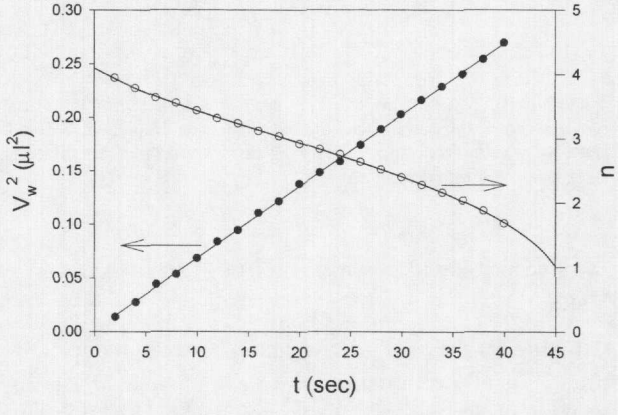

FIGURE 9. Hexadecane droplet in a polypropylene yarn, the current wicking volume squared and the ratio $n = R_d/R_y$ as functions of time.

calculated. Table II gives the estimated structural parameters of the yarns. The errors in the estimated ε and R values are mainly due to the non-uniformity of capillary sizes in the yarn and the uncertainty in the measured yarn radius. Figure 10 shows the dependence of the wicking time T_w as a function of the square of initial droplet volume squared V_0^2 for wicking of hexadecane droplets of different sizes in nylon yarns. The estimated structural parameters of the yarns are also given in Table II. The values of porosity ε and hydraulic radius R are quite reasonable.

TABLE II. Estimated structural parameters of the yarns.

Liquid	Yarn	Slope, s/mm^6	R_y, μm	ε	R, μm
Hexadecane	nylon	185	91 ± 4	0.24 ± 0.07	8 ± 3
Hexadecane	PP, #1	149	102 ± 4	0.28 ± 0.07	5 ± 2
PP-912	PP, #2	1050	100 ± 4	0.26 ± 0.07	11 ± 3

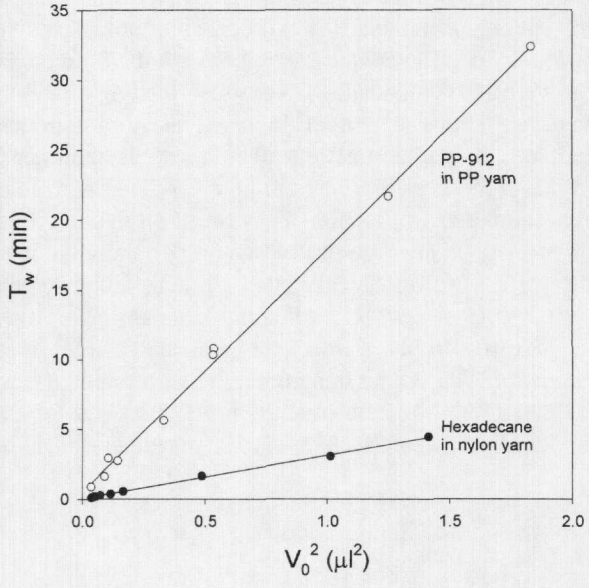

FIGURE 10. Time of droplet absorption as a function of the initial droplet volume squared for wicking of hexadecane droplets of different sizes by a nylon yarn and for wicking of PP-912 droplets of different sizes by a polypropylene yarn.

WICKING OF SPIN FINISH PP-912 IN POLYPROPYLENE YARNS

Figure 10 shows a linear relation between the wicking time T_w and the initial droplet volume squared V_0^2 for wicking of droplets of the spin finish PP-912 in a polypropylene yarn (PP, #2). The contact angle of PP-912 with PP fibers was determined by the Wilhelmy method [7, 9] as $\cos\theta_a = 0.837$, indicating a partial wetting situation. The model works as well for the partial wetting as for the complete wetting. The estimated structural parameters of the yarn are also included in Table II.

Conclusions

In this paper, we have studied the wicking kinetics of liquid droplets into yarns using a computerized imaging system. We suggest a new method for characterizing the yarn structure based on a comparative analysis of the time needed for complete droplet absorption as a function of initial droplet volume for various yarns. We develop a model to describe wicking kinetics, and we show that for wetting liquids, the capillary pressure at the liquid front dominates the Laplacian pressure caused by the droplet curvature. As a result, the droplet is sucked into the yarn in accordance with the Lucas-Washburn equation. The time of droplet absorption T_w is a linear function of the initial droplet volume squared V_0^2. For a given liquid-yarn pair, the slope of this relation provides important information about the yarn properties. We have verified the linear relationship between T_w and V_0^2 with experimental data. For nonwetting liquids, the model predicts that droplet wicking can still occur even if θ_a is greater than 90°. However, the relation between T_w and V_0^2 becomes nonlinear. Currently, we are conducting experimental work aimed at confirming the theoretical criterion for forced spreading of nonwetting fluids.

Appendix: Carroll's Formulas for Droplet Parameters

Figure 2 shows the profile of a liquid droplet residing on a horizontally placed cylindrical fiber or yarn. If both the yarn diameter and droplet size are sufficiently small, the effect of gravity on the droplet shape is negligible. The equilibrium condition for the droplet is that the curvature is constant everywhere on the droplet surface. The droplet is symmetrical around the yarn axis. The left and right sides of the droplet are also mirror symmetrical.

The droplet shape can be described by four parameters: the radius of the yarn R_y, the maximum radius of the droplet R_d, the droplet length along the yarn L_d, and the contact angle that the droplet makes with the yarn θ. For any point (z, x) on the droplet surface, Carroll [1] derived the following equation for the droplet profile:

$$z = \pm R_y[aF(\varphi, m) + nE(\varphi, m)] \quad , \qquad \text{(A1)}$$

where $F(\varphi, m)$ and $E(\varphi, m)$ are the elliptic integrals of the first and second kind, respectively, n, a, and m are defined as

$$n = R_d/R_y \quad , \tag{A2}$$

$$a = \frac{n \cos\theta - 1}{n - \cos\theta} \quad , \tag{A3}$$

$$m = 1 - a^2/n^2 \quad , \tag{A4}$$

and φ is calculated by

$$\varphi = \arcsin\left[\frac{1 - x^2/R_d^2}{m}\right]^{1/2} \quad , \tag{A5}$$

where x is the radius at the point (z, x) on the droplet surface. When $x = R_y$, the droplet length is given by

$$L_d = 2|z| = 2R_y[aF(\varphi, m) + nE(\varphi, m)] \quad . \tag{A6}$$

Carroll also derived the equation for the total volume V_t of the droplet and the section of yarn surrounded by the droplet:

$$V_t = \frac{2\pi n R_y^3}{3}[(2a^2 + 3an + 2n^2)E(\varphi, m) - a^2F(\varphi, m) + (n^2 - 1)^{1/2}(1 - a^2)^{1/2}] \quad . \tag{A7}$$

The net volume of the droplet V_d can be calculated by subtracting the volume V_y of the yarn section surrounded by the droplet:

$$V_d = V_t - V_y = V_t - \pi R_y^2 L_d \quad . \tag{A8}$$

The Laplace excess pressure ΔP of the droplet is given as follows:

$$\Delta P = (2H)\gamma = \frac{2(n - \cos\theta)}{R_y(n^2 - 1)}\gamma \quad , \tag{A9}$$

where $2H$ is the droplet curvature.

If we put $\cos\theta = 1$, the model can be significantly simplified. That is, only the ratio $n = R_d/R_y$ specifies the geometric parameters of the droplet. In Equations A1, A6, and A7, because of the identity $\varphi = \pi/2$, the elliptic integrals $F(\varphi, m)$ and $E(\varphi, m)$ are replaced by the complete elliptic integrals $K(m)$ and $E(m)$, respectively.

Literature Cited

1. Carroll, B. J., The Accurate Measurement of Contact Angle, Phase Contact Area, Drop Volume, and Laplace Excess Pressure in Drop-on-Fiber Systems, *J. Colloid Interface Sci.* **57**(3), 488–495 (1976).
2. Chidambaram, P. R., Lanning, B., and Edwards, G. R., A Simple Capillary Rise Apparatus to Measure Wettability in Metal-Ceramic Systems, *Rev. Sci. Instrum.* **16,** 3839–3843 (1994).
3. Johnson, R. E., Jr., and Dettre, R. H., Wettability and Contact Angles, in "Surface and Colloid Science," vol. 2, E. Matijevic′, Ed., J. Wiley & Sons, NY, 1969, pp. 85–153.
4. Kamath, Y. K., Hornby, S. B., Weigmann, H.-D., and Wilde, M. F., Wicking of Spin Finishes and Related Liquids into Continuous Filament Yarns, *Textile Res. J.* **64**(1), 33–40 (1994).
5. Kissa, E., Wetting and Wicking, *Textile Res. J.* **66**(10), 660–668 (1996).
6. Lucas, R., Ueber das Zeitgesetz des kapillaren Aufstiegs von Flussigkeiten, *Kolloid Z.* **23,** 15–22 (1918).
7. Miller, B., Experimental Aspects of Fiber Wetting and Liquid Movement Between Fibers, in "Absorbency," P. K. Chatterjee, Ed., Elsevier, NY, 1985, pp. 121–147.
8. Minor, F. W., Schwartz, A. M., Wulkov, E. A., and Buckles, L. C., Migration of Liquids in Textile Assemblies, *Textile Res. J.* **29,** 931–939 (1959).
9. Penn, L. S., and Miller, B., A Study of the Primary Cause of Contact Angle Hysteresis on Some Polymeric Solids, *J. Colloid Interface Sci.* **78**(1), 238–241 (1980).
10. Perwuelz, A., Mondon, P., and Caze, C., Experimental Study of Capillary Flow in Yarns, *Textile Res. J.* **70**(4), 333–339 (2000).
11. Rahli, O., Tadrist, L., Miscevic, M., and Santini, R., Fluid Flow Through Randomly Packed Monodisperse Fibers: The Kozeny-Carman Parameter Analysis, *J. Fluid Eng. Trans. ASME* **119**(3), 188–192 (1997).
12. Skelton, J., Interfiber Forces During Wetting and Drying, *Science* **190**(10), 15–20 (1975).
13. Washburn, E. W., The Dynamics of Capillary Flow, *Phys. Rev.* **17,** 273–283 (1921).

Manuscript received December 15, 2000; accepted May 8, 2001.